Aerospace Science and Technology ••• (••••) •••–•••

Contents lists available at ScienceDirect

Aerospace Science and Technology

www.elsevier.com/locate/aescte

Comparison of box-wing and conventional aircraft mission performance using multidisciplinary analysis and optimization

Stephen A. Andrews [a], Ruben E. Perez [b,*]

[a] X Computational Physics, Los Alamos National Laboratory, Mail Stop P365, P.O. Box 1663, Los Alamos, NM 87545 USA
[b] Department of Mechanical and Aerospace Engineering, Royal Military College of Canada, Kingston, ON, K7K 7B4, Canada

ARTICLE INFO

Article history:
Received 5 March 2018
Received in revised form 31 May 2018
Accepted 31 May 2018
Available online xxxx

Keywords:
Box-wing
Multidisciplinary optimization
Aircraft design
Unconventional aircraft

ABSTRACT

Box-wing aircraft designs have the potential to achieve significant reductions in fuel consumption. Closed non-planar wing designs have been shown to reduce induced drag and the statically indeterminate wing structure can lead to reduced wing weight. In addition, the streamwise separation of the two main wings can provide the moments necessary for static stability and control, eliminating the weight and aerodynamic drag of a horizontal tail.

Proper assessment of the disciplinary interactions in box-wing designs is essential to determine any realistic performance benefits arising from the use of such a configuration. This study analyzes both box-wing and conventional aircraft designed for representative regional-jet missions. A preliminary parametric investigation shows a lift-to-drag ratio advantage for box-wing designs, while a more detailed multidisciplinary study indicates that the requirement to carry the mission fuel in the wings leads to an increase of between 5% and 1% in total fuel burn compared to conventional designs. However, the multidisciplinary study identified operating conditions where the box-wing can have superior performance to conventional aircraft despite the fuel volume constraint.

1. Introduction

The box-wing planform geometry is a nonplanar wing design which can achieve significant reductions in induced drag per unit of planform area [1]. The box-wing geometry consists of two main lifting surfaces connected at their tips by a third, near vertical, lifting surface, see Fig. 1. In addition to aerodynamic benefits, the closed, nonplanar wing design forms a statically indeterminate structure which may lead to a lighter wing [2]. If the two main lifting surfaces of the box-wing design have sufficient longitudinal separation, they can create the moments necessary for stability along this axis and eliminate the need for a horizontal tail as well as its associated structural weight and aerodynamic drag.

An unconventional nonplanar wing geometry presents a conceptual design challenge, as analysis tools used at the conceptual stage may not capture all the *physics processes* [4] which influence the performance of the aircraft. In addition, as no box-wing transport aircraft has entered service, there is no obvious initial point in the design space of the box-wing geometries to investigate.

Earlier investigations of aircraft with a box-wing planform have considered one or two of these important design disciplines in isolation. A thorough review of previous work on box-wing aircraft is given by Cavallaro and Demasi [5]. The box-wing aircraft design was first proposed by Prandtl in 1918 [6]. Further theoretical investigations were performed by von Kármán and Burgers [7]. These two studies sought the planform shape with the lowest induced drag (neglecting airfoil section effects) given a fixed span and maximum separation between wings. This optimum planform shape was a box-wing with a spanwise circulation distribution where equal lift was carried on each wing and the spanwise loading on the horizontal surfaces was a combination of a constant circulation plus elliptical distribution with the circulation decreasing linearly along the vertical segments, as shown in Fig. 2. More recent studies have claimed that this is not the only spanwise loading which can achieve minimum induced drag [8,9]. These authors showed that the constant component of the spanwise circulation can vary between the fore and aft wings while still achieving minimum induced drag, allowing the two horizontal wings to generate different lift forces. The effects of parasitic drag and the complex flow which develops at the joints between lifting surfaces were examined in two studies which performed a high-fidelity aerodynamic shape optimization of box-wing designs [10,11]. These studies showed that box-wings can have approximately a 7% advantage in fuel consumption in the cruise phase of the mission [11].

* Corresponding author.
E-mail address: Ruben.Perez@rmc.ca (R.E. Perez).

https://doi.org/10.1016/j.ast.2018.05.060
1270-9638/

Nomenclature

Subscripts

1	Fore wing
2	Aft wing
α	Sensitivity to angle of attack ..... /deg
n	Sum of fore and aft wings

Dimensionless groups

C_D	Aircraft drag coefficient
C_L	Aircraft lift coefficient
C_l	Local lift coefficient
C_W	Aircraft weight coefficient
Re	Reynolds number
C_d	Airfoil drag coefficient
$C_{d_{p_0}}$	Airfoil section constant parasitic drag coefficient
$C_{d_{p_1}}$	Airfoil section linear parasitic drag coefficient
$C_{d_{p_2}}$	Airfoil section quadratic parasitic drag coefficient
$C_{l_{max}}$	Airfoil section maximum lift coefficient
C_{l_o}	Airfoil section lift coefficient at zero incidence
C_m	Airfoil section pitching moment coefficient
Ma	Mach number

Acronyms

BLF	Balanced Field Length ..... ft (0.305 m)
C2OEICG	Second segment OEI climb gradient
MTOW	Maximum Takeoff Weight ..... lb_f (4.44 N)
OEI	One Engine Inoperative
SFC_T	Thrust specific fuel consumption 1/s
TSSL	Sea-level standard day thrust ..... lb_f (4.44 N)

Variables

$\Delta_{c.g.}$	Center of gravity offset ..... ft (0.305m)
γ	Wing twist angle, relative to aircraft centerline ... deg
λ	Wing taper
ρ	Density ..... slug/ft^3 (516 kg/m^3)
b	Total span ..... ft (0.305 m)
$\bar{c}$	Mean aerodynamic chord ..... ft (0.305 m)
h	Height between lifting surfaces ..... ft (0.305 m)
L	Lift ..... lb_f (4.44 N)
n_{pan}	Number of vortex panels
n_{seg}	Number of wing segment
S	Projected Area ..... ft^2 (0.0930 m^2)
V	Airspeed ..... ft/s (0.305 m/s)
W	Weight ..... lb_f (4.44 N)
$x_{1\to 2}$	Stagger between lifting surfaces ..... ft (0.305 m)
a	Speed of Sound ..... ft/s (0.305 m/s)
α_{mvr}	Aircraft angle of incidence in maneuver ..... deg
α_o	Incidence at zero airfoil section lift ..... deg
f_m	Aerodynamic meta-model
G	Constraint function
g	Vector of constraints
R	Mission range ..... nmi (1.85 km)
T	Thrust ..... lb_f (4.44 N)
V	Volume ..... ft^3 (0.0283 m^3)
$W_{n.g.}$	Weight carried by nose landing gear ..... lb_f (4.44 N)
x	Vector of design variables

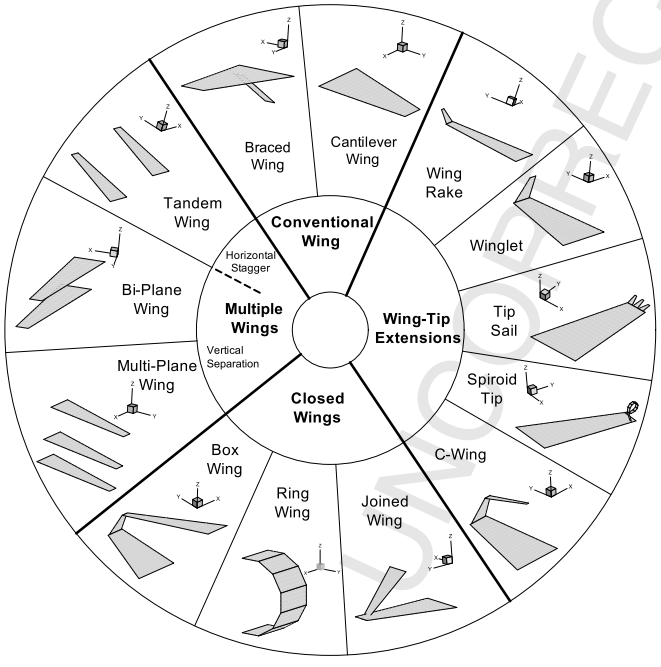

Fig. 1. Different nonplanar wing designs. Box-wings are a member of the closed nonplanar wing family [3].

Previous studies which compared the weight of a conventional wing to a joined-wing design showed that when the weight of the main lifting surfaces were compared, the joined-wing did not provide a significant advantage in terms of structural weight [12,13]. However, if the joined-wing was designed such that the horizontal tail could be removed, the total weight of the aircraft's lifting

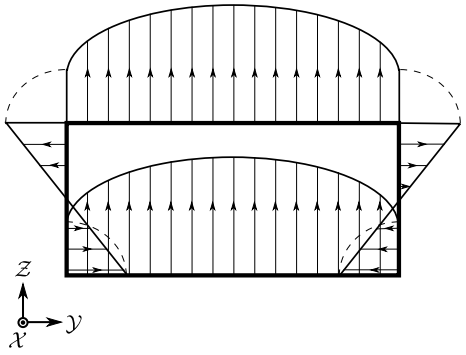

Fig. 2. Optimal spanwise lift distribution for a box-wing aircraft. Adapted from Prandtl [6].

surfaces was reduced. A similar result was found when the wing structure of box-wing designs was considered [14]. This shows an important interaction between the analysis of longitudinal stability and structural weight in box-wing aircraft. When considering the couplings between the disciplines of aerodynamics and structures alone, it was found that the box-wing had a 5% advantage in mission fuel consumption, compared with a conventional design [15].

Previous work has shown that the requirements of static longitudinal stability may impose an aerodynamic penalty on the box-wing design [16]. This study, however, used an induced drag model that may have been overly sensitive to lift imbalance between both wings compared to more recent models [8,9]. Preliminary studies have also been performed on the dynamic stability of box-wing aircraft and have shown that designs which were statically stable would have acceptable handling qualities with a stability augmentation system [17].

Other important questions in the design of a box-wing aircraft have been considered by previous studies including fuel capacity [18,19], high-lift device allocation [20] and landing gear placement [18]. No previous studies, however, have examined the performance and interaction between all these design disciplines in a single analysis nor considered how the box-wing design would affect the fuel consumed over the various phases of a typical mission.

The wide range of possible box-wing planform geometries and the many interacting disciplines required to assess the performance of such designs makes a thorough search of the entire box-wing design space challenging. To address this challenge, the present study takes a two-step approach. First, a parametric investigation considered a wide range of box-wing geometries, locating designs which are optimal only with respect to their lift-to-drag ratio and longitudinal stability. The best design from this parametric study is used as the initial point for a more comprehensive multidisciplinary optimization. This optimization uses a combination of existing aircraft design methods as well as new models developed for the box-wing configuration. This multidisciplinary study considers a wider range of interdisciplinary couplings than previous investigations and evaluates the aircraft performance and design constraints across the course of the mission. The study also considers how any advantages provided by the box-wing configuration are affected by the choice of mission. Two different box-wing aircraft are considered, each designed for a different payload and range taken from representative regional-jet missions. The objective of the optimization is to minimize the fuel consumed during the mission. To make an unbiased comparison between existing aircraft and box-wing designs, the optimized box-wing aircraft are compared to conventional aircraft with the same mission, whose designs are also optimized using the same procedure. Both the conventional and box-wing aircraft are designed for a regional-jet mission. Previous work has shown that the box-wing is best suited to such short range missions. The potential savings in structural weight of the box-wing had the greatest effect on short-range aircraft where the structural weight makes up a larger fraction of the Maximum Takeoff Weight than for long-range designs [3]. Additionally, short-range aircraft spend a greater fraction of their mission in the climb and descent phases, where lower induced drag is advantageous.

Section 2 presents the methodology and results of the parametric study. Section 3 discusses the formulation of the multidisciplinary problem as well as the models used to predict the performance of box-wing and conventional aircraft. The results of this multidisciplinary problem are shown in Section 4 for both box-wing and conventional aircraft. Conclusions are given in Section 5.

2. Parametric study

A parametric study is performed to gain a better understanding of how the geometry of the box-wing aircraft affects its aerodynamic performance, quantified by lift-to-drag ratio. This study, similar to that performed in [21], varies three key geometric parameters and examines optimized designs constrained to achieve static longitudinal stability at cruise conditions. For each planform geometry in the parametric study, there exists a twist distribution along the wing which maximizes the lift-to-drag ratio while meeting stability, trim and maneuverability requirements at cruise. A constrained optimization is needed for each geometry considered in this study in order to determine this distribution. The optimized box-wing results are compared to a conventional cantilevered wing with an optimized twist distribution. The design of this reference wing is similar to an existing regional-jet transport aircraft, the Bombardier CRJ-200 [22]. Both the box-wing and reference wing share the same planform area as well as cruise conditions and lift requirement, given in Table 1.

Table 1
Reference aircraft characteristics.

Total wing area	587.1	ft^2 (0.093 m^2)
Aspect ratio	8.9	–
Maximum takeoff weight	47000	lb_f (4.44 N)
Fuselage length	80.0	ft (0.305 m)
Cruise Mach	0.74	–
Cruise altitude	37000	ft (0.305 m)
Maneuver altitude	25000	ft (0.305 m)

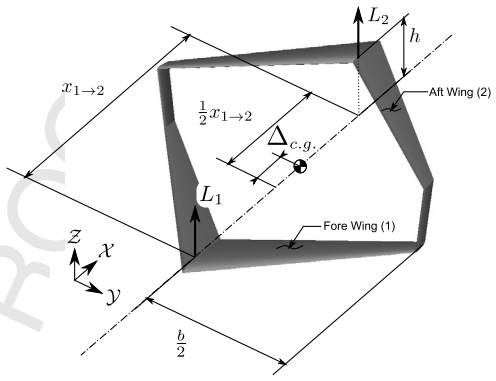

Fig. 3. A generic box-wing geometry with important dimensions labeled. The stagger is $x_{1\to2}$, the center of gravity offset is $\Delta_{c.g.}$. The vertical separation between wings is h, the total span is b, the fore wing area is S_1, the aft wing area S_2 and the total planform area is S_n.

2.1. Parametrization of the box-wing geometry

Three parameters are considered in this study: the stagger of the wings, the height-to-span ratio, and the relative area of the fore wing. Stagger is measured as the distance between the quarter chord point of the fore and aft wings. The total area of the wings remains constant but the allocation of the area between the fore and aft wings is variable. These dimensions are shown for a generic box-wing aircraft in Fig. 3. The analysis tools used in this study are not able to account for buckling and aero-structural effects, which become more pronounced for slender wings. The aspect ratio of the wing with the smallest planform area is kept equal to that of the reference aircraft so that optimal solutions are practical when the wing structure is considered.

The ranges of the three parameters for the study are shown in Table 2. The bounds are chosen to encompass the range of wing designs which can be integrated into the reference aircraft. The upper limit of stagger is chosen so that the fore and aft wings can be attached to the reference aircraft's fuselage. A previous analytic study on the effects of box-wing geometry on longitudinal stability provided initial guidance on possible ranges of the fore-to-aft wing area ratio [23]. Designs with area ratios less than 0.4 could not perform a critical 2.5 g maneuver as the fore wing was too highly loaded. The possibility also existed that designs with a smaller aft wing may have performance advantages. Therefore, the bounds of 0.4 and 0.6 were chosen as they should encompass the best box-wing configurations.

The aerodynamic forces and moments on the aircraft are evaluated by a vortex panel aerodynamic model which is able to solve for the induced drag of the nonplanar box-wing design. More details of this model are given in Section 3.3. The parasitic drag of the airfoils is evaluated using a fixed drag polar, evaluated for a NACA 23012 airfoil at a Reynolds number of 1×10^7 and a Mach number of 0.74. The airfoil section properties are given in Table 3.

Table 2
Ranges of the parameters used in the study.

Parameter	Bounds	
	Lower	Upper
h/b	0.125	0.5
$2x_{1\to2}/b$	0.5	2.0
S_1/S_n	0.4	0.6

Table 3
Reference airfoil section properties.

Zero-lift incidence	α_o	−2.015	deg
Zero incidence lift	C_{l_o}	0.221	–
Section pitching moment coefficient	C_m	−0.0096	–
Constant parasitic drag coefficient	$C_{d_{p0}}$	0.0081	–
Linear parasitic drag coefficient	$C_{d_{p_1}}$	0.0010	–
Quadratic parasitic drag coefficient	$C_{d_{p_2}}$	0.0059	–
Maximum section lift coefficient	$C_{l_{max}}$	1.2	–

The sweep of the box-wing is determined by the stagger. The sweep angle is defined so that the fore wing is sweeping aft and the aft wing is sweeping forward such that the leading edge of the fore and aft wing tips are aligned. The fore and aft wings have different taper ratios so that both wings have the same chord at the wing-tip. The taper of the smallest wing is an optimization variable. Box-wing geometries with different combinations of the three main parameters in this study are shown in Fig. 4.

2.2. Optimization problem

Each geometry in the parametric study has a unique optimal twist distribution. A constrained optimization problem is given in (1) to determine this optimal distribution while maintaining static longitudinal stability and trim.

$$\max \frac{C_L}{C_D}$$
$$\text{such that} \begin{cases} 1.0\text{ g} & \begin{cases} C_L = C_W \\ C_m = 0 \\ -\frac{C_{m_\alpha}}{C_{L_\alpha}} > 0.07 \end{cases} \\ 2.5\text{ g} & \begin{cases} C_L = 2.5 C_W \\ C_{l,i} < C_{l_{max\,i}} - 0.05 \quad \{i \in 1 \ldots n_{pan}\} \end{cases} \end{cases} \tag{1}$$
$$\text{with respect to } \left\{ \gamma_i \{i \in 1 \ldots n_{seg}+1\},\ \frac{\Delta_{c.g.}}{\bar{c}},\ \alpha_{mvr},\ \lambda \right.$$

The box-wing model consists of five lifting segments, n_{seg}, whose twist angle, γ_i, can be set at both the root and the tip. The twist distribution is continuous along the wing so that there are six independent twist values. The first value sets the twist of the fore wing at its root and the sixth value sets the wing root twist of the aft wing. In addition to the wing twist angles, the optimization problem has three other variables. The center of gravity offset, $\Delta_{c.g.}$, is needed to meet the stability constraints. The offset is defined as in Fig. 3; a positive offset represents movement of the center of gravity aft of the midpoint between the quarter-chord point of the fore and aft wing. The taper, λ, of the smallest wing is a variable in order to meet the maneuverability constraints which are critical at the wing tip. The maneuver incidence, α_{mvr}, is also a variable. The ranges and initial estimates for these variables are shown in Table 4.

The problem is constrained so that the wing generates sufficient lift at cruise and maneuver conditions. The 2.5 g maneuver is performed at the 'maneuver altitude' given in Table 1 which was the highest altitude where the reference aircraft could perform a sustained 2.5 g maneuver. Longitudinal stability is enforced by constraining the design to have zero pitching moment at cruise and a static margin of 7%. The static margin limit is typical of transport aircraft [24,25]. The problem is also constrained so that no wing

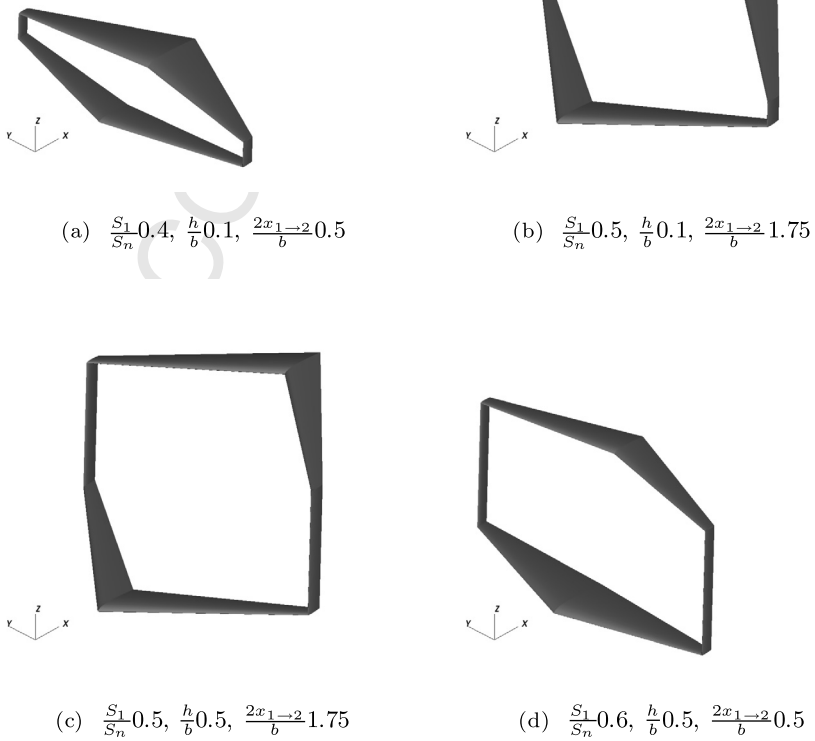

(a) $\frac{S_1}{S_n}0.4,\ \frac{h}{b}0.1,\ \frac{2x_{1\to2}}{b}0.5$ (b) $\frac{S_1}{S_n}0.5,\ \frac{h}{b}0.1,\ \frac{2x_{1\to2}}{b}1.75$

(c) $\frac{S_1}{S_n}0.5,\ \frac{h}{b}0.5,\ \frac{2x_{1\to2}}{b}1.75$ (d) $\frac{S_1}{S_n}0.6,\ \frac{h}{b}0.5,\ \frac{2x_{1\to2}}{b}0.5$

Fig. 4. Representative box-wing geometries. The taper of the smallest wing was 0.325 for all designs.

Please cite this article in press as: S.A. Andrews, R.E. Perez, Comparison of box-wing and conventional aircraft mission performance using multidisciplinary analysis and optimization, Aerosp. Sci. Technol. (2018), https://doi.org/10.1016/j.ast.2018.05.060

Table 4
Variable bounds and initial values for the optimization problem.

		Lower bound	Upper bound	Initial value
$\gamma_i \{i \in 1 \ldots n_{seg}+1\}$	[deg]	−20.0	20.0	1.0
$\frac{\Delta_{c.g.}}{\bar{c}}$	[–]	−2.0	2.0	0.0
α_{mvr}	[deg]	0.0	20.0	2.5
λ	[–]	0.2	1.0	0.4

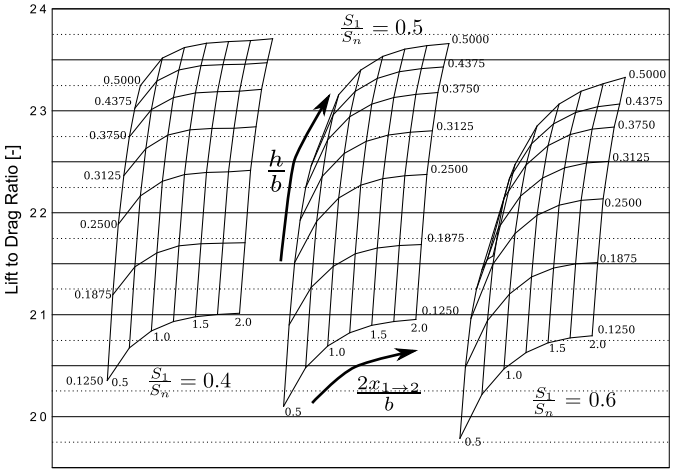

Fig. 5. Parametric study of box-wing geometry with static longitudinal stability and trim constraints. Parameters are: Normalized fore wing area, $\frac{S_1}{S_n}$, Normalized quarter-chord stagger $\frac{2x_{1\to2}}{b}$ and height-to-span ratio $\frac{h}{b}$.

panel exceeded its maximum local lift coefficient while performing the 2.5 g maneuver.

The optimization problem given by (1) is solved by the gradient-based SQP optimization algorithm, `SNOPT` [26], implemented in the `pyOpt` optimization framework [27].

2.3. Results

2.3.1. Reference wing

The wing from the reference aircraft is modeled as an isolated wing with a planar, trapezoidal planform. The three angles making up the reference wing's twist distribution, as well as the wing's taper, are optimized using the same problem formulation as the box-wing designs. The stability constraints are not enforced as the horizontal tail of the reference aircraft is not modeled.

The lift-to-drag ratio of the wing in isolation is 26. However, the wing requires a horizontal tail to maintain static stability which creates induced, parasitic and trim drag. As the box-wing is designed to cruise with zero pitching moment, it was assumed that the reference aircraft is likewise designed so that, at the start of cruise, the horizontal tail generates no lift. Therefore, an additional drag term is added to the reference wing to account for the parasitic drag of the horizontal tail. This contribution to the wing's total drag is estimated using the analytic method presented in [28]. The parasitic drag of the horizontal tail reduces the lift-to-drag ratio of the reference wing to 22.14.

2.3.2. Box-wings

The results of the parametric study are shown in Fig. 5 as a carpet plot. The single dependent variable is the lift-to-drag ratio of the box-wing designs. The lift-to-drag ratio of the reference wing and horizontal tail is shown as a horizontal line. Designs with large stagger and a height-to-span ratio of 0.25 or greater have superior aerodynamic performance to the reference aircraft, showing that even when the requirements of static stability are considered, many box-wing designs are superior to conventional aircraft.

Previous studies, which considered the effects of height-to-span ratio on the induced drag of a box-wing design, concluded that the induced drag of a wing decreases continuously with increasing separation, asymptotically approaching half the induced drag of a monoplane [6]. Results from the present study, shown in Fig. 5 display a similar trend despite the increased wetted area introduced by the vertical wing segments as the height-to-span ratio increases. The increased wetted area only penalizes the design at height-to-span ratios greater than 0.5.

The highest lift-to-drag ratios are obtained by designs with area ratios of 0.4 and 0.5 with the largest values of stagger. These trends can be better understood by considering the findings from a recent study on the stability of tandem wing designs [23]. This study used an analytic model of inviscid flow over a tandem-wing to understand how the planform geometry of such designs affects longitudinal stability as well as lift-to-drag ratio while remaining trimmed [23]. In this earlier study, tandem wing designs with the fore wing making up 0.4 times the total planform obtained the highest lift-to-drag ratio while maintaining trim and static stability. In the present parametric study, the best wing with an area ratio of 0.4 ($\frac{L}{D} = 23.69$) also had a slight advantage over the best design with area ratio 0.5 ($\frac{L}{D} = 23.64$). In both these studies the lift-to-drag ratio was also seen to increase with increasing stagger.

The impact of stagger on the lift-to-drag ratio in both the present study and the previous work of Andrews and Perez [23] is unexpected in light of Munk's stagger theorem which states that the induced drag of a dual wing configuration does not change with stagger, *provided the circulation distribution on both wings remains the same* [29]. Though Munk's theorem was originally developed for planar wings modeled as a lifting line, the theorem is more generally applicable to nonplanar wing shapes. Stagger has an effect on the lift-to-drag ratio of the aircraft when trim requirements are considered. Since the aircraft is constrained to have a positive static margin of 7%, the center of gravity is located ahead of the aerodynamic center of the aircraft. This creates a pitching moment which must be canceled by changing the lift generated by the fore and aft wings, invalidating the assumptions of Munk's stagger theorem. Increasing stagger increases the effective moment arm of each wing when canceling out the pitching moment imposed by the stability requirement.

The present results show that the relationships derived for tandem wing designs, with no vertical surface connecting the fore and aft wings, also apply to the more complex geometry of the box-wing aircraft. In addition, considering the parasitic drag on the wing did not alter these conclusions. These results also agreed well with a high-fidelity aerodynamic optimization of a box-wing aircraft which showed that the optimal wing design had an area ratio of 0.44 [11].

This parametric study identified several important trends in the design of box-wing aircraft. First, the area allocation between the fore and aft wings should be somewhere between 0.4 and 0.5. Second, the stagger should be increased as much as possible to reduce the impact of the trim constraint on the lift-to-drag ratio of the designs. Third, increasing the height-to-span ratio of the wings increases lift-to-drag ratio of box-wing designs and allows such designs to achieve higher lift-to-drag ratios than conventional configurations.

These guidelines were developed considering only the interactions between aerodynamic performance and static longitudinal stability. Further disciplinary analyses must be considered to determine if the aerodynamic advantages of the box-wing design will translate into reduced fuel consumption during a realistic mission. The following sections will use the findings from this study to inform a more comprehensive analysis of the box-wing configuration.

Please cite this article in press as: S.A. Andrews, R.E. Perez, Comparison of box-wing and conventional aircraft mission performance using multidisciplinary analysis and optimization, Aerosp. Sci. Technol. (2018), https://doi.org/10.1016/j.ast.2018.05.060

3. Multidisciplinary analysis

The results of the preceding analysis show that there are box-wing designs which are superior to a conventional cantilevered wing when assessed on the basis of the lift-to-drag ratio of the wings while constrained to maintain acceptable longitudinal stability properties. The purpose of the multidisciplinary analysis is to determine if these advantages persist when additional disciplines are considered and the fuel required to complete a typical transport mission is used as the metric for comparison. The additional disciplines considered in this study impose constraints on the design in addition to those considered in the previous section. The effects of these constraints can erode the performance advantages which the parametric study showed the box-wing enjoyed compared to a conventional aircraft. The fuel burnt over the course of a mission is a quantity that is of greater interest to aircraft operators than lift-to-drag ratio when comparing aircraft designed for a transport mission. Sections 3.1 through 3.8 discuss the computational models used to analyze the box-wing aircraft design. A description of the optimization problem and the optimization algorithm is given in Section 3.9.

An additional factor considered in the multidisciplinary study is the effect of mission range and payload. Since mission ranges and payloads are linked to the design of transportation networks [28], these are not considered as independent variables. Rather, a short and long range regional jet mission are chosen to be representative of two in-service aircraft, the Bombardier CRJ-200 and CRJ-900. Designs using the shorter-ranged mission are referred to as 50 passenger aircraft and designs using the longer-ranged mission are referred to as 86 passenger aircraft. For each mission, a baseline design with a conventional planform is optimized with a fixed planform shape derived from published data for the aircraft [22]. Two corresponding box-wing designs are also optimized, given the same mission range and payload as these baseline aircraft.

3.1. Geometric parametrization

The planform shape of the box-wing aircraft is parameterized in the same manner as in the study described in Section 2. However, additional geometric parameters are needed to describe systems which the parametric study did not consider. These three systems are: high-lift devices, landing gear, and propulsion. The locations of the high-lift devices are shown in Fig. 6. The high-lift devices are located between fixed inboard and outboard stations. The outboard limit is set to allow space for ailerons to be attached to the wing. Since the CRJ-200 aircraft does not have slats installed, slats are only included in the 86 passenger box-wing. Both the 50 and 86 passenger box-wing have plain trailing edge flaps. The size of the high-lift devices is determined by two variables, the percentage of the total planform area covered by flaps and the ratio of the flap area on the fore wing to the aft. The baseline aircraft use single slotted flaps and the fixed flap sizes are taken from [22]. The box-wings used plain flaps so that they could also be used as elevators.

The landing gear for the box-wing designs is attached to the fuselage, while the landing gear location for the conventional design is constrained to remain attached to the wing. The landing gear location is defined by three variables, the axial location of the nose and main gear as well as the strut length of the main gear and the distance outboard of the fuselage of the main gear. These variables are shown in Fig. 6.

The propulsion system will be discussed further in Section 3.4. The axial location of the engine inlet is variable to allow the engine to move for trim purposes.

The payload is modeled as two concentrated weights for passengers and baggage. The weight of the passengers is located at the center of the cabin area and the weight of the baggage is located at the center of the baggage compartment door. Weights for the passengers and baggage are 185 lbf/pax(823 N/pax) and 35 lbf/pax (156 N/pax), respectively [30,25].

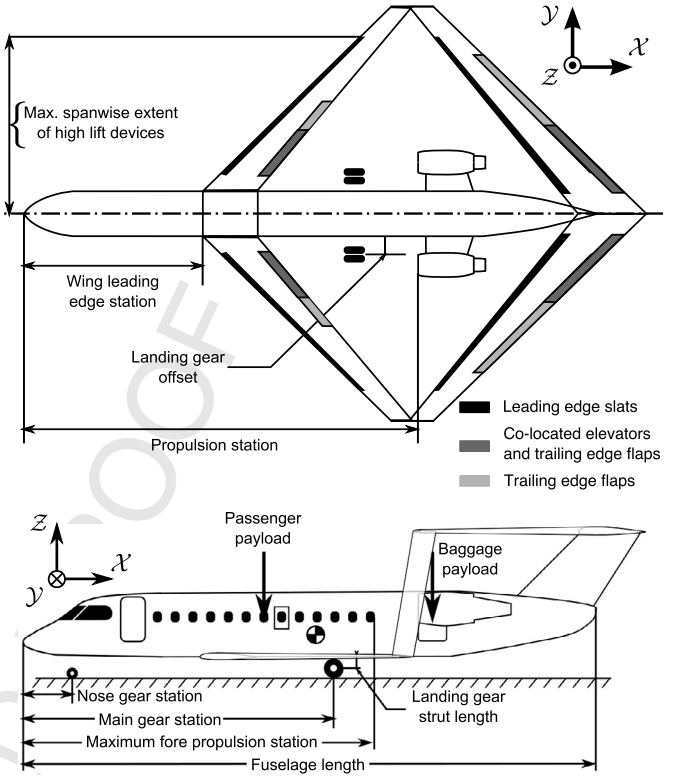

Fig. 6. Geometry of the box-wing aircraft used in the multidisciplinary optimization.

Table 5
Mission specifications.

Property	Units	Passengers	
		50	86
Start of cruise altitude [22]	ft $\times 10^2$ (0.0305 km)	370	370
Cruise Mach number [22]	–	0.74	0.78
Range [22]	nmi (1.85 km)	965	1540
Fuselage length [22]	ft (0.305 m)	88	119
Takeoff field length [22]	ft (0.305 m)	5010	6140
Engine bypass ratio	–	6.2	5.0

3.2. Mission performance

Two different mission specifications are considered, that of a short range and of a long range regional jet. The generic mission profile is shown in Fig. 7 and details of the mission specifications are given in Table 5.

Unlike the parametric study, which considered only the two performance points of cruising and maneuvering flight, the multidisciplinary study ensures that the aircraft can complete a representative transport mission. Fuel burn and thrust requirements for each phase of the mission are determined by a mission performance model described by both Jansen [28] and Andrews [31].

This performance model considers phases of the mission other than cruise. Of greatest interest to total mission fuel consumption are takeoff, climb, and cruise. The takeoff performance uses the method of Powers [32] to calculate Balanced Field Length (BFL). The fuel consumed in the climb phase of the mission is determined by numerical integration of the aircraft equations of motion over

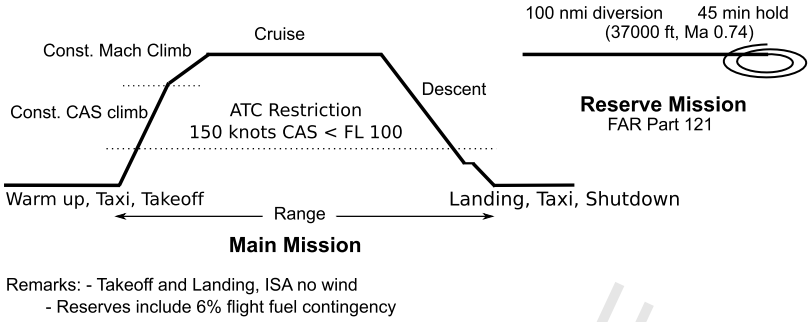

Fig. 7. The standard mission profile.

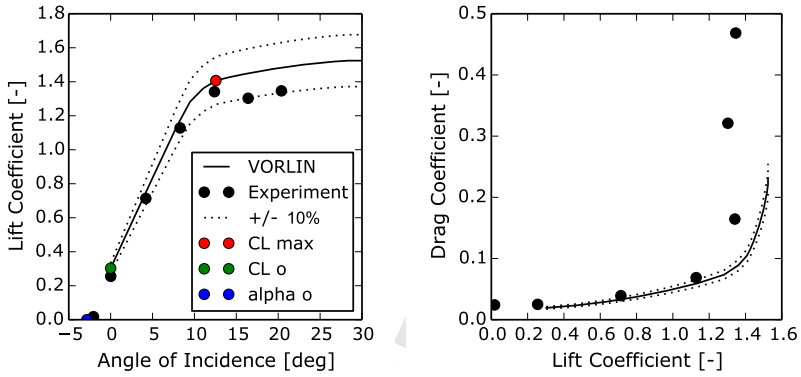

(a) Lift curve (b) Drag polar

Fig. 8. Validation example of the pyVORLIN code using the NASA supercritical-wing transport model [37].

fixed steps in altitude. The Breguet range equation is used to solve for the fuel consumption in cruise.

3.3. Aerodynamics

The inviscid flow over the wing is modeled using a vortex panel solver (Section 3.3.1) while the profile and parasitic drag of the airfoil sections is calculated *a priori* and added to each vortex panel based on the local Reynolds number (Section 3.3.2). This aerodynamic model takes an approach similar to that of Gallay and Larendeau [33]. Though this approach is able to solve for the aerodynamic forces acting on the aircraft on the order of seconds, a meta-model is needed for the numerical integration of the aircraft equations of motion used for the climb and descent phases of the mission (Section 3.3.4).

3.3.1. Vortex panel solver

The cruise and maneuvering aerodynamic performance is calculated using a vortex panel aerodynamic solver, `pyVORLIN`. This solver discretizes the wing into a series of spanwise panels with only one chordwise panel. Each of these wing panels is attached to a single wake panel which extends 100 span lengths downstream. The algorithm used to determine the local circulation distribution along the wing given this arrangement of vortex panels is described in [34]. Given the circulation distribution, lift and drag were calculated by taking the sum of the streamwise and the normal-to-streamwise components of the local forces generated on each vortex panel.

This approach allows the induced drag to be solved directly but additional contributions to the drag require section data for the airfoil. The local circulation and Reynolds number at each spanwise panel is used to obtain the section properties of the airfoil. Using the local circulation rather than the installation angle of the airfoil to determine the effective airfoil incidence allows the three-dimensional effects of the finite wing to influence the airfoil section properties.

The wave-drag effects on the wing are modeled using the Korn equation [35].

Validation studies for conventional and joined wing aircraft are given by Andrews [31,36]. These studies consider tandem-wing, joined-wing and conventional aircraft and the vortex panel analysis showed good agreement to wind-tunnel data. One of these validation studies, for the NASA Supercritical-Wing transport model [37], is shown in Fig. 8. These results show the lift curve (Fig. 8(a)) and drag polar (Fig. 8(b)) for the aircraft in cruise configuration at Mach 0.168. The lift and drag were predicted well in the pre-stall regime which was where all designs in the present study operated.

3.3.2. Airfoil model

The airfoil properties used to determine the effects of camber and parasitic drag in `pyVORLIN` are obtained by interpolation from tables of airfoil properties calculated at Mach 0.3 for a range of eight Reynolds numbers between 1×10^6 and 1×10^8. Airfoil section properties are evaluated using the code VGK [38]. This couples a finite difference solution to the inviscid flow over the airfoil to models of boundary layer growth along the airfoil's surface. This allows the code to model the performance of airfoil sections in viscous, compressible flow.

3.3.3. High-lift device and control surface modeling

The use of high-lift devices and control surfaces adds additional components to the airfoil section drag, lift, pitching moment and maximum lift coefficient. These adjustments to the section properties are estimated based on the equations given by Roskam [39]. Operation in ground effect is simulated by adding a mirror image of the vortex panels, reflected across the ground plane. Validation

Please cite this article in press as: S.A. Andrews, R.E. Perez, Comparison of box-wing and conventional aircraft mission performance using multidisciplinary analysis and optimization, Aerosp. Sci. Technol. (2018), https://doi.org/10.1016/j.ast.2018.05.060

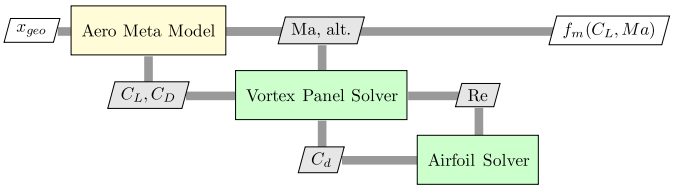

Fig. 9. XDSM diagram of the aerodynamic meta-model.

examples of both high-lift devices and operation in ground effect are given by Andrews [31].

3.3.4. Aerodynamic meta-model

The aircraft performance model described in Section 3.2 uses numerical integration of the aircraft equations of motion to solve the takeoff, climb and descent phases of the mission. This requires on the order of one hundred evaluations of the aerodynamic forces on the aircraft which presented a prohibitive computational cost. A meta-model of aerodynamic forces was developed which performed linear interpolation on a grid of Mach numbers and altitudes between takeoff and cruise conditions. An XDSM diagram [40] shows how the meta-model interacts with the vortex panel solver and airfoil model to create the tables of lift and drag corresponding to different operating conditions (see Fig. 9). The meta-model was validated by comparing the mission fuel burn computed using this model to the results obtained when using the vortex panel solver. The meta-model reduced computational time by 96% and introduced an error of 0.1% in fuel burn across the mission. More details of this model's formulation are given in Andrews [31].

3.4. Propulsion

The installed sea level thrust of the fuselage mounted engines in the baseline and box-wing designs was a variable in the optimization. A model was needed to relate the variable sea-level static thrust and the constant bypass ratio of the engine to the expected performance of the engine across the mission. Such a model has been proposed by Bartel and Young [41] and was calibrated to match modern gas-turbine performance data. This model relates the sea level maximum thrust and bypass ratio to available thrust and specific fuel consumption at a given Mach number and altitude. According to the authors of this model, it was able to predict maximum thrust at a given altitude and Mach number within ±4% and was able to predict specific fuel consumption within ±0.5% [41]. Effects of partial throttle settings are accounted for using relations from Mattingly [42].

3.5. Structural weight

The weight of all the aircraft components other than the wing are evaluated using models based on historical data. These equations are taken from previous studies on aircraft component weight estimation [43–46]. Ranges for the center of gravity location for each component are obtained from Chai et al. [47]. Further details of how each component's weight was estimated are given in Andrews [31].

Since the box-wing is an unconventional structure, existing wing weight models cannot be used to predict its weight. An equivalent beam fully stressed structural model, described by Andrews et al. [2] is used to estimate the weight of the wing. This code determines the weight of a fully stressed wing considering static aerodynamic forces at critical combinations of altitude and loading. Comparison against other conceptual design tools showed that this model is as good as existing approaches for estimating the weight of conventional aircraft and is able to model the statically indeterminate structure and unusual distribution of aerodynamic forces found in box-wing aircraft [2].

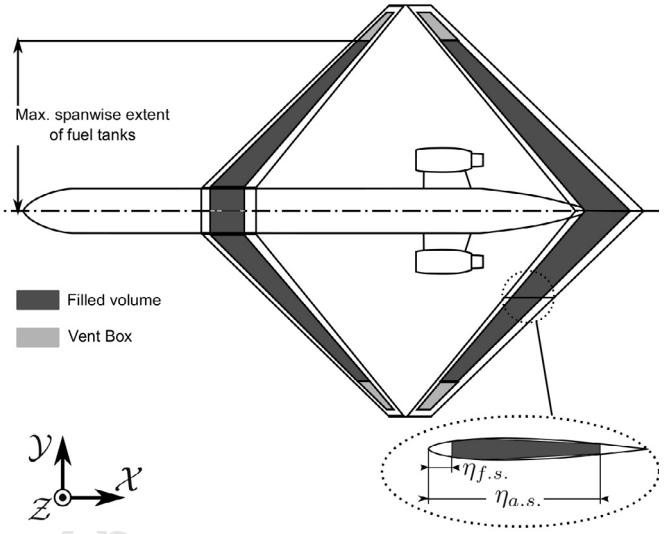

Fig. 10. Fuel tank locations for the box-wing aircraft.

The fully stressed structural model represents the wing as an airfoil-conforming hexagonal wing-box composed of direct stress carrying booms at each vertex, connected by shear stress carrying skins. This model is sensitive to the thickness of the airfoil as well as the location of the fore and aft spar. These spar locations are variables in the multidisciplinary optimization and are shown in Fig. 10.

3.6. Stability

The multidisciplinary study considers a wider range of stability and control constraints on the design than the parametric study. Stability is assessed with both full and empty fuel tanks to ensure the aircraft remained stable as fuel was consumed. The aircraft is constrained to be trimmed in level flight at the start of cruise with full fuel tanks.

In addition to considering stability in cruise, the longitudinal stability is considered at rotation speed in ground effect immediately after the wheels leave the ground.

In addition to considering the stability in ground effect, the aircraft is constrained to rotate on takeoff with an elevator deflection of less than 20 degrees. The equations of motion for the aircraft at takeoff rotation are taken from Roskam [48] and consider the effects of the aerodynamic forces and moments of the wing, the mass and inertia of the aircraft, the thrust of the engines as well as the moment generated by the deflected elevator. Conventional aircraft have the advantage that their all-moving tail can be inclined at takeoff to increase the aircraft pitching moment. As the installation angles of the box-wing aircraft were fixed, the aircraft can only use control surface deflections to create aerodynamic moments on takeoff.

3.7. Landing gear

The location of the landing gear imposes several important constraints on the design which impact structural weight and aircraft stability. The tip back constraint ensures that the main landing gear is located sufficiently aft of the aircraft center of gravity that the aircraft will not tip back on its tail when on the ground. The tip-over constraint ensures that the aircraft will not tip on its side while maneuvering on the ground. The tail strike constraint ensures that the tail will not contact the ground during normal takeoff rotation.

Please cite this article in press as: S.A. Andrews, R.E. Perez, Comparison of box-wing and conventional aircraft mission performance using multidisciplinary analysis and optimization, Aerosp. Sci. Technol. (2018), https://doi.org/10.1016/j.ast.2018.05.060

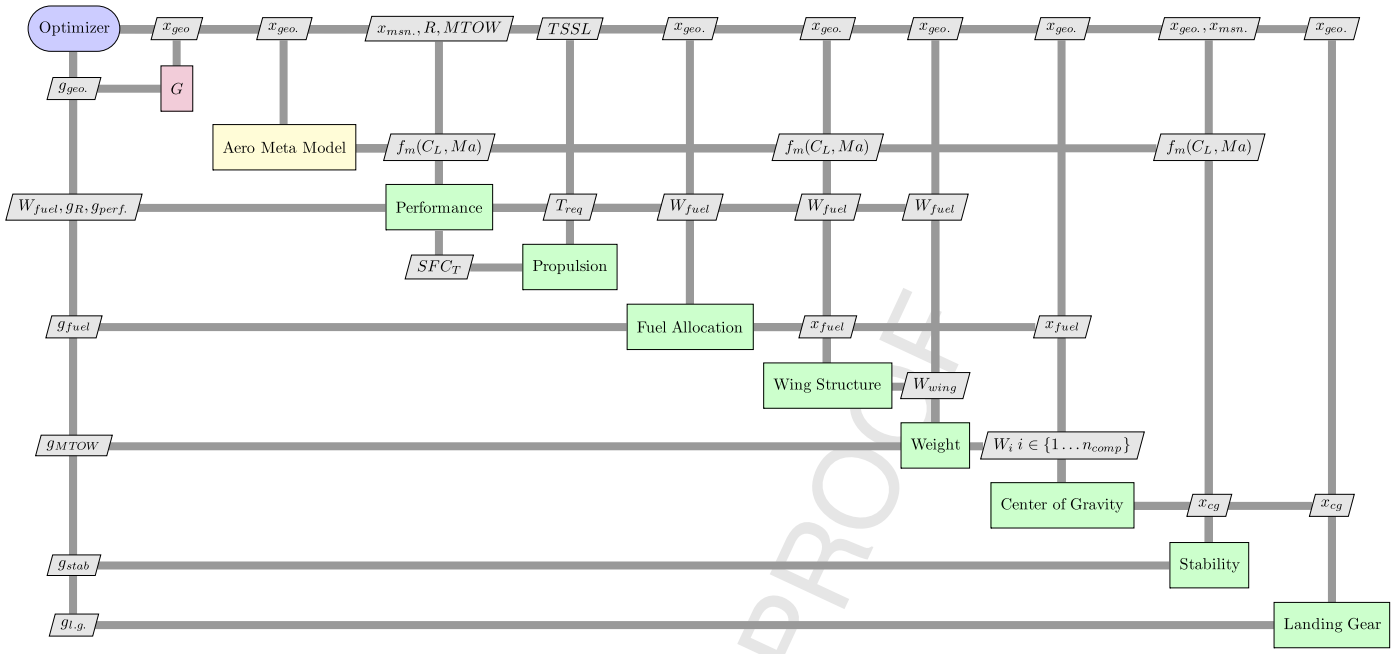

Fig. 11. Flow of information in the multidisciplinary problem.

The nose gear was located so that it carried between 5% and 20% of the aircraft's weight. The lower limit ensured that the nose gear would have sufficient traction to steer the aircraft.

3.8. Fuel volume

The fuel tanks are located within the wings of the aircraft and in the fuselage where the wing box passes through, as seen in Fig. 10. Additional fuel storage in the fuselage is not considered due to certification requirements as well as challenges integrating fuel tanks into the cabin design. The fuel tanks are modeled as a frustum of a hexagonal pyramid with the thickness derived from the airfoil section profile. The fore and aft locations of the tank are the spar locations used by the wing weight model. The available fuel volume, adjusted for the internal structure of the wing, is an important parameter in the design of the box-wing aircraft and will be discussed in subsequent sections.

3.9. Optimization problem

The multidisciplinary optimization seeks an aircraft configuration with the lowest fuel consumption over the course of the mission while meeting all the constraints placed on the design due to performance, safety and airport operation requirements.

The previous sections described the various disciplinary analyses needed to determine the aircraft fuel consumption and evaluate the constraints on the design. These analyses are not independent; each depends on the results of one or more disciplinary analysis. The flow of information from one analysis to another is structured to minimize the number of interdisciplinary conflicts. This ordering is shown in Fig. 11 as an XDSM diagram [40]. There are some couplings, however, which cannot be resolved and require an Interdisciplinary Feasible (IDF) approach [49]. The Maximum Takeoff Weight (MTOW) of the aircraft and the distance traveled in cruise (Range) are two variables on which many of the analyses depend but cannot not be calculated *a priori*. The IDF approach introduces two new variables to represent these unknown quantities, and equality constraints are added to the optimization problem to ensure that the variables matched the results of the analysis when the problem was feasible.

3.9.1. Variables

The lists of design variables and their ranges for both the conventional and box-wing aircraft are given in Appendix A. The initial values for these variables are chosen based on the results from the parametric study in Section 2. For variables not considered in the parametric study, assumed values are chosen that yielded a feasible initial point for the optimization. The upper and lower bounds are chosen to be as wide as possible while remaining within the regime where the disciplinary analyses are valid. For some variables there are clear bounds based on the geometry of the aircraft. For other variables, large bounds which would never be active are chosen. One important bound is the limit of the aspect ratio of the smallest wing. This is set to 10 as wings with a higher aspect ratio could be susceptible to aeroelastic effects which the structural analysis cannot model. The structural analysis was validated using a set of aircraft designs with known wing weights; the largest aspect ratio considered in this validation study was 10 [2].

3.9.2. Constraints

The constraints imposed on the design of both the baseline and box-wing aircraft are shown in Table 6. There are four primary groups of constraints: interdisciplinary coupling, geometric, stability and performance. The interdisciplinary coupling constraints are needed to ensure that the unknown quantities provided to the multidisciplinary analysis, shown in Fig. 11 matched the outputs of the analysis. In addition to the geometric constraints given in Table 6, the box-wing has further geometric constraints imposed on the design. The aft wing is constrained to intersect either the fuselage or vertical tail in order to ensure that the forces and moments generated by this wing can be transmitted to the fuselage. The leading edge of the root of the forward wing cannot extend forward of the cabin door location of the baseline aircraft to ensure that the aircraft can be serviced by existing airport equipment. In addition, the maximum spanwise extent of the box-wing is constrained so that it meets FAA airport gate area guidelines [50].

The performance constraints in Table 6 ensure that the aircraft is able to complete all phases of the mission. The balanced field length constraint ensures the box-wing aircraft can operate in the same airports as the baseline aircraft. The second segment climb gradient with one engine inoperative (C2OEICG) is a certification

Please cite this article in press as: S.A. Andrews, R.E. Perez, Comparison of box-wing and conventional aircraft mission performance using multidisciplinary analysis and optimization, Aerosp. Sci. Technol. (2018), https://doi.org/10.1016/j.ast.2018.05.060

Table 6
Constraints common to baseline and box-wing aircraft.

Interdisciplinary coupling constraints	
Cruise lift	$C_L = C_W$
Maneuver lift	$C_{L_{mvr}} = 2.5C_W$
MTOW	$\text{MTOW}_{in} = \text{MTOW}$
Mission range	$R_{in} = R$
Geometric constraints	
Twist rate	<2.0 deg/ft (6.55 deg/m)
Landing gear constraints (with and without fuel, aft c.g.)	
Tip back angle [51]	>15.0 deg
Tail strike angle [51]	>10.0 deg
Tip over angle [51]	<63.0 deg
Minimum Ground clearance	>2 ft (0.61 m)
Nose loading	$0.05 < \frac{W_{n.g.}}{\text{MTOW}} < 0.2$
Stability constraints	
Cruise stability constraints (with and without fuel, fore and aft c.g.)	
Static stability	$0.07 < -\frac{C_{m_\alpha}}{C_{L_\alpha}}$
Negative pitch stiffness	$C_{m_\alpha} < 0$
Trimmable	$0 < C_{m_o}$
Cruise trim constraint (with fuel, fore c.g.)	
Trimmed	$C_m = 0$
Takeoff constraints (with fuel, fore and aft c.g.)	
No autorotation	Pitching moment with no elevator deflection is negative at rotation speed
Takeoff rotation	Pitching moment with full elevator deflection greater than forces resisting rotation
Takeoff stability	$0.04 < -\frac{C_{m_\alpha}}{C_{L_\alpha}}\Big\vert_{takeoff}$
Performance constraints	
Balanced field length	BFL <1.1 times the value in Table 5
Takeoff second segment OEI CG	C2OEICG > 0.024
Fuel volume	$V_{avail} > V_{req}$
Maneuver C_l margin	$C_{l_i} < C_{l_{max}} \{i \in 1..n_{pan}\}$

requirement taken from Raymer [25] and is imposed on both box-wing and baseline designs. The fuel volume constraint ensures that the mission fuel could fit in the aircraft wing. Both aircraft had to perform a 2.5 g maneuver at the altitude given in Table 1. The wing is constrained so that the local lift generated on each vortex panel does not exceed the maximum lift coefficient for the airfoil section.

3.9.3. Optimizer

The optimization problems is solved using the SNOPT optimizer [26], implemented in the pyOpt framework [27]. The initial point for the geometric parameters is taken from the parametric study described in Section 2. Though the SNOPT algorithm is, in general, able to tolerate an initially infeasible point, the multidisciplinary problem formulation was sufficiently complex so that the SNOPT algorithm would not achieve proper convergence if the initial point were not feasible. To find a feasible initial point, some design variables which cannot be estimated from the parametric study or from published data were iterated until the constraints were feasible.

4. Results

Each of the four optimization problems for the baseline and box-wing designs for the 50 and 86 passenger mission were optimized using the procedure described in Section 3.9.

4.1. Baseline aircraft

An initial check of the aircraft design procedure described in Section 3 is to compare the performance of the optimized 50 and 86 passenger baseline aircraft to published values for the CRJ aircraft, on which these designs were based. This comparison is shown in Table 7. With the exception of the installed thrust on the 86 passenger baseline aircraft, the published values are in good agreement with the predicted values. The most critical point for engine sizing is the requirement to maintain a minimum rate of climb of 2.5 ft/s (0.762 m/s) at the cruise Mach number and altitude. The model of Bartel and Young [41] discussed in Section 3.4 may not predict the thrust lapse with altitude properly, resulting in over-sized engines installed on the 86 passenger aircraft. This extra thrust at sea level contributes to the decreased takeoff field length for the 86 passenger aircraft. Though the engines are over-sized compared to the real aircraft, the predicted Operational Empty Weight and Maximum Takeoff Weight remain in good agreement, indicating that the variable of interest in this study, fuel burn, is well predicted.

4.2. Overall comparison of box-wing to baseline

Having established that the optimization and analysis procedures are able to predict the performance of in-service aircraft, a comparison of the optimized baseline aircraft to the box-wing aircraft is made based on the metrics of their aerodynamic performance, total fuel consumption and their structural weight.

The data in Table 8 show that both the 50 and 86 passenger box-wing aircraft achieve a higher value of lift-to-drag ratio at cruise than conventional aircraft. This confirms the findings of previous studies of box-wing transport aircraft which concluded that there was an aerodynamic advantage in this configuration. However, when the actual weight of fuel required for the mission was compared to the baseline designs, the box-wing designs burn more fuel over the course of the mission. The principal reason for the performance deficit is the significant increase in planform area. This is caused by the requirement that the mission's fuel be stored in the wings. The entire available fuel volume in the wings is used for fuel storage. The increased planform area also leads to increased wing weight, giving the baseline aircraft an advantage over box-wing designs for both Operating Empty Weight, and Maximum Takeoff Weight, despite the fact that the box-wing does not require a horizontal stabilizer.

As noted by previous authors [1], the low induced drag of the box-wing leads to a slightly shorter Balanced Field Length for the box-wing designs, despite the increased takeoff weight. The optimal design variables in Tables A.10 and A.11 show that both the

Table 7
Comparison of multidisciplinary optimization results with published data for baseline reference aircraft [22]. 'Diff' is the value from the model less the published value normalized by the published value.

		CRJ 200			CRJ 900		
		Jane's	Model	Diff.	Jane's	Model	Diff.
Passengers	–		50			86	
Range	nmi (1.85 km)		940			1540	
MTOW	lb_f (4.44 N)	47500	47500	+0.2%	80500	81500	+1.3%
OEW	lb_f (4.44 N)	30300	29600	−2.1%	47500	46400	−2.3
Thrust	lb_f (4.44 N)	9220	9380	+1.7%	13100	15600	+19%
BFL	ft (0.305 m)	5010	5100	+1.7%	6140	5560	−9.4%

Table 8
Comparison of conventional (CRJ) and box-wing (NPL) aircraft for the 50 and 86 passenger mission. 'Diff.' is the value from the box-wing less the value for the baseline normalized by the value for the baseline.

		50-pax			86-pax		
		Baseline	Box-wing	Diff.	Baseline	Box-wing	Diff.
Cruise L/D	–	15.8	16.1	+2.0%	16.3	17.4	+6.2%
Fuel weight	lb_f (4.44 N)	5630	5910	+5.0%	13600	13800	+1.6%
Planform area	ft^2 (0.0930 m^2)	587	727	+24%	739	1120	+51%
Total wing weight	lb_f (4.44 N)	4550	7290	+60%	7340	12600	+72%
OEW	lb_f (4.44 N)	29600	33100	+12%	46400	53600	+16%
MTOW	lb_f (4.44 N)	47500	51400	+8.0%	81500	88600	+8.7%
BFL	ft (0.305 m)	5100	5040	−1.1%	5559	5460	−2.1%
Height-to-span	–	–	0.308		–	0.250	
Stagger	$/\frac{1}{2}b$	–	0.890		–	0.957	
Fore wing area	$/S_n$	–	0.500		–	0.498	

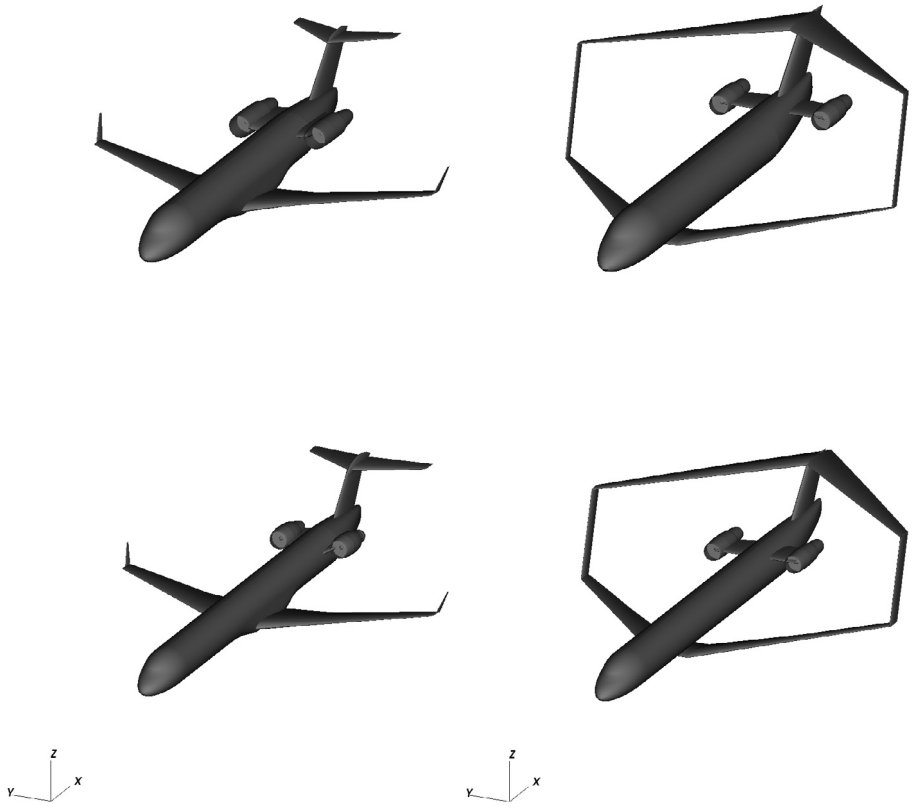

(c) 86 passenger baseline (d) 86 passenger box-wing

Fig. 12. Comparison of optimized baseline and box-wing aircraft geometries.

baseline and box-wing achieved these field lengths with effectively no installed flaps. The box-wing designs are constrained to have the same takeoff field length as the baseline aircraft. Since the fuel constraint increased the planform area of the wings significantly, the designs could meet this constraint without flaps.

The isometric views of the optimized box-wing and baseline aircraft are shown in Fig. 12.

4.3. Aerodynamic performance

Two different comparisons between the box-wing and the baseline aircraft's aerodynamic performance can be made. First the dimensionless Mach-lift-to-drag ratio for both the 50 and 86 passenger box-wing designs is shown in Figs. 13(a) and 13(b). The data are presented as a "sky map" [52] where contours of Mach-lift-to-drag are plotted between the physical limits of where the aircraft can operate. At high speeds, the aircraft is limited by a maximum dynamic pressure of 350 lb_f/ft^2 (16.8 kPa). This is the dynamic pressure acting on the baseline aircraft at 1.15 times the cruise speed at the maneuvering altitude in Table 1. At low speeds, the aircraft is limited by the wing stalling. The wing is considered to have stalled when a single vortex panel exceeds its maximum local lift coefficient. At high altitudes the aircraft is limited by the engine's available power.

The importance of the Mach-lift-to-drag ratio can be seen in (2) which shows how the fuel fraction for the cruise segment was calculated.

$$\frac{W_{fuel}}{W_{cruise}} = \left(1 - \exp\left(\frac{-R \cdot \mathrm{SFC}_T}{a\mathrm{Ma}\,(C_L/C_D)_{L=W}}\right)\right) \tag{2}$$

The product $a\ \mathrm{Ma}\frac{C_L}{C_D}$ is in the denominator of the exponential term, the sound speed, a is constant for a fixed altitude. As this ratio increases, the value of the exponent will tend towards one.

Please cite this article in press as: S.A. Andrews, R.E. Perez, Comparison of box-wing and conventional aircraft mission performance using multidisciplinary analysis and optimization, Aerosp. Sci. Technol. (2018), https://doi.org/10.1016/j.ast.2018.05.060

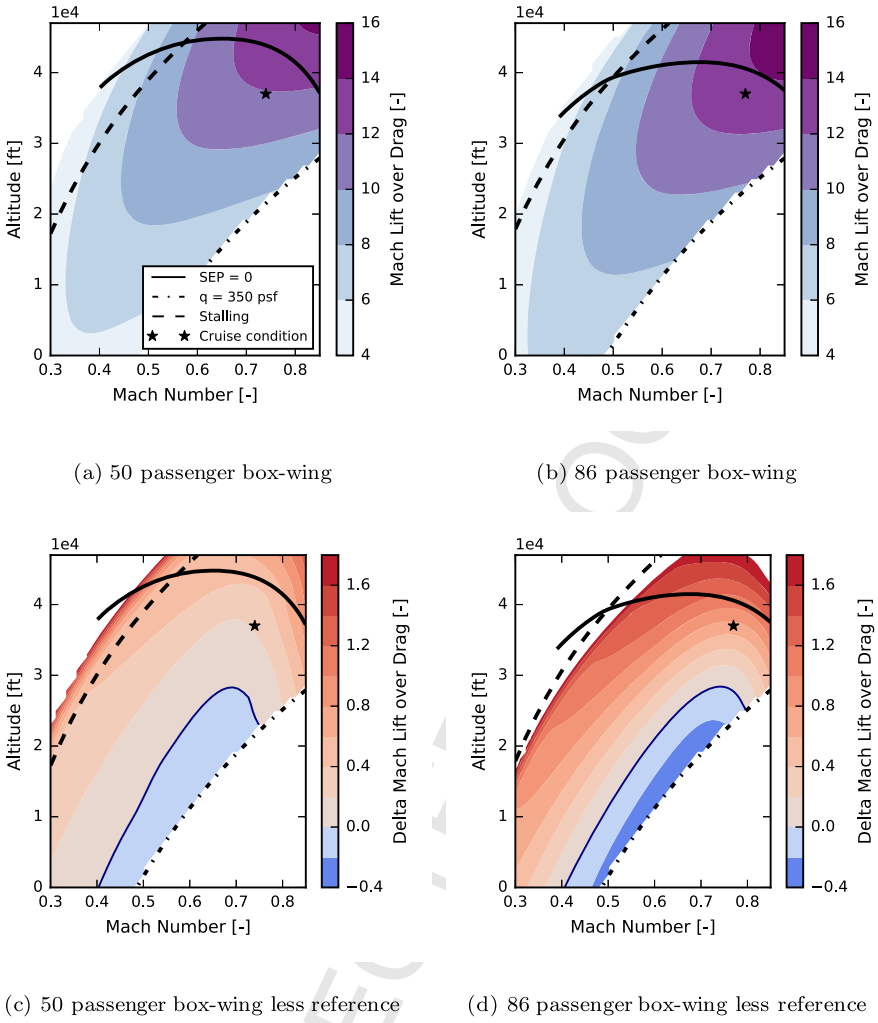

(a) 50 passenger box-wing

(b) 86 passenger box-wing

(c) 50 passenger box-wing less reference

(d) 86 passenger box-wing less reference

Fig. 13. Sky-maps showing the Mach-lift-to-drag ratio of both aircraft sizes.

Large values of the product of Mach number and the lift-to-drag ratio leads to a smaller fraction of the aircraft weight at the start of cruise being burnt as fuel.

Within the bounds where the aircraft could safely operate, both the 50 and 86 passenger aircraft cruise near their maximum attainable Mach-lift-to-drag values. In Figs. 13(c) and 13(d), the difference between the Mach-lift-to-drag values of the box-wing aircraft and the baseline designs are shown with a positive value indicating an advantage for the box-wing. Both box-wing designs show an advantage in Mach-lift-to-drag compared to the baseline design at cruise conditions.

The aerodynamic advantage of the box-wing aircraft disappears, however, when a dimensional quantity rather than the dimensionless Mach-lift-to-drag ratio is examined. Figs. 14(a) and 14(b) show the total drag, in lb_f on both the baseline and box-wing aircraft for a range of steady, level flight conditions occurring over a range of Mach numbers at the cruise altitude. From Table 8, the 50 passenger box-wing has a 24% greater wing area than the baseline design. Despite the advantages in Mach-lift-to-drag shown in Fig. 13, when this increased wing area is taken into account, the 50 passenger box-wing has inferior performance to the baseline aircraft across the entire range of Mach numbers investigated. Though the 86 passenger aircraft does not have an advantage in total drag compared to the baseline aircraft at cruise conditions, this design generates less drag than the baseline aircraft at speeds less than Mach 0.65. Despite a significantly larger projected area than the baseline aircraft, the box-wing design yields significant reductions in induced drag which compensate for the increased parasitic drag across all speeds.

4.4. Aircraft performance

The Specific Air Range (SAR) for an aircraft represents the distance traveled per lb_f (4.4 N) of fuel. Unlike the Mach-lift-to-drag ratio, the SAR depends on the weight of the aircraft and thus penalizes the box-wing aircraft which has a larger planform area. The specific air range for the box-wing aircraft, as well as the difference between the box-wing and baseline aircraft are shown in Fig. 15 with the same bounds and sign conventions as in Fig. 13.

The higher drag force for the 50 passenger box-wing compared to the baseline leads to the 50 passenger box-wing having a lower specific air range than the baseline throughout its operating envelope. This means that for all operating conditions, the 50 passenger box-wing burns more fuel than the baseline aircraft.

Though the 86 passenger box wing also has a lower specific air range than the baseline design at cruise conditions, there is a large area of the "sky-map" in Fig. 15(d) where the box-wing has a greater specific air range than the baseline aircraft. If the mission were modified so that the aircraft could cruise in this favorable region, the box-wing would have a lower fuel burn than a baseline

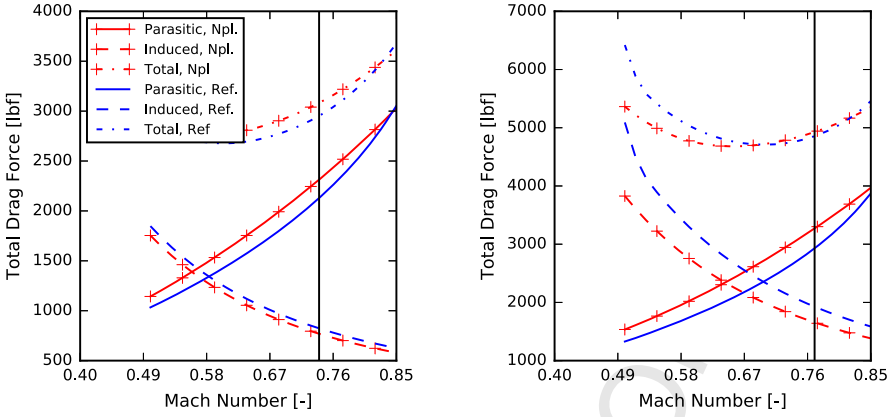

(a) 50 passenger (b) 86 passenger

Fig. 14. Comparison of drag forces in lb_f (4.4 N) of the box-wing to the baseline aircraft for the 50 and 86 passenger missions over a range of Mach numbers at the cruise altitude. The vertical line represents the cruise Mach number.

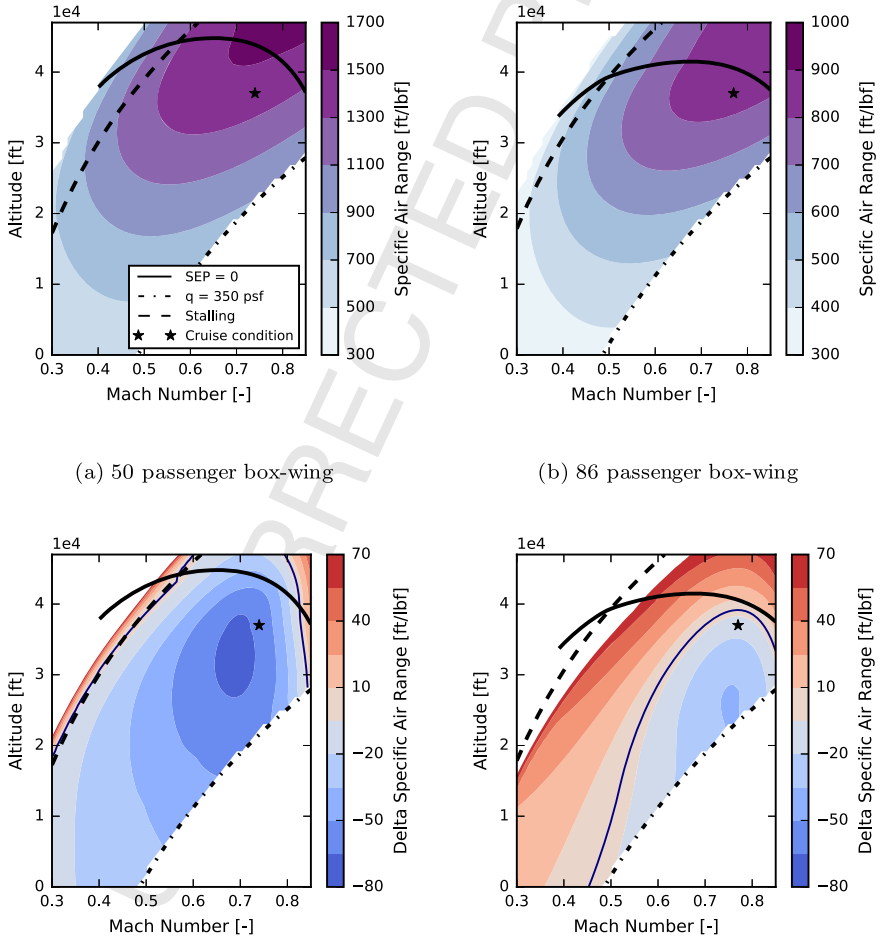

(a) 50 passenger box-wing (b) 86 passenger box-wing

(c) 50 passenger box-wing less reference (d) 86 passenger box-wing less reference

Fig. 15. Sky maps showing the specific air range in ft/lbf (1.35 m/N) for both aircraft sizes.

design cruising at the same conditions. Such a mission, however, may not be able to be integrated into an air transportation network and considering the implications of optimizing the mission along with the aircraft design would require a broader analysis of how a box-wing transport would fit into such a network [28].

4.5. Active variable bounds

Several of the variable bounds were active in the optimized box-wing designs. The following sections examine the effects that these bounds had on the optimal solution.

4.5.1. Fore wing location

In the parametric study, the lift-to-drag ratio was seen to increase with increasing separation of the two wings. This separation is limited in the case of the 50 passenger box-wing by the presence of the forward cabin door. To allow the aircraft to be serviced by existing airport infrastructure, the fore wing cannot extend forward of the main cabin door location. This operational constraint limits the lift-to-drag ratio of the 50 passenger box-wing. This shows the importance of considering a wide range of operational constraints in multidisciplinary studies of aircraft design.

4.5.2. Aspect ratio

For the shorter range box-wing design, the aspect ratio variable bound is active, and is almost reached for the longer range box-wing design. The span of the wing is already constrained by airport gate constraints. However, if the span of the 50 passenger box-wing were set to the gate constraint and had the same total area as the baseline wing, evenly divided between fore and aft wings, each wing would have an aspect ratio of 21. The upper limit on the aspect ratio variable is needed to prevent the optimizer from exploiting the fact that the disciplinary analyses do not account for aeroelastic effects which become critical at high aspect ratios. Limiting the aspect ratio ensures a fair comparison between the baseline and box-wing aircraft designed for the same mission. However, when this upper limit of the aspect ratio is increased to 15 and a new optimization is performed on the 86 passenger aircraft with this new bound, the 86 passenger aircraft has a 10% fuel burn advantage over the baseline aircraft despite still having a larger planform area. However, this fuel burn advantage is relative to the baseline aircraft with an aspect ratio of seven. If the baseline design were allowed to also adopt a larger aspect ratio, then the box-wing may not have such a large advantage. This finding was corroborated by a recent high fidelity aerodynamic shape optimization study of a box-wing aircraft. This aircraft was also designed for a short-range regional jet mission [11]. The optimal box-wing design in this study also had an active fuel volume constraint and a planform area 21% greater than the baseline aircraft in that study. The box-wing had an aspect ratio of 16.7 compared to the baseline design of 8.9 and a 7% fuel burn advantage. The available fuel volume in the wing was based on the entire wing's internal volume and did not account for the location of the fore and aft spars. These results show that box-wing designs can have superior performance to conventional aircraft if the box-wing is allowed to adopt large aspect ratios. This also shows that the fuel volume constraint caused the box-wing designs to have a larger planform area than the baseline aircraft.

4.6. Active constraints

4.6.1. Fuel volume

The constraint which had the greatest impact on the design of box-wing aircraft was the fuel constraint. If the thickness-to-chord ratio of the wings remains constant, and if the chord of a single main wing is divided in two to make a box-wing design of the same projected area, the resulting cross section available for fuel storage is divided in half.

To see the effect of the fuel storage requirements, a new optimization was performed on the 86 passenger box-wing aircraft with this constraint removed. The initial projected area of the box-wing is equal to the baseline design and the original aspect ratio limit of 10 was used. The results of this optimization are shown in Table 9. In this case, the box-wing design has a 1.2% advantage over the baseline aircraft in terms of total fuel consumed over the course of the mission. However, there is a significant volume of fuel in the box-wing aircraft which cannot be stored in the wing.

Table 9
Comparison of a 86 passenger baseline and box-wing aircraft with and without the fuel volume constraint.

		Baseline	Box-Wing	Diff.
MTOW	lb_f (4.4 N)	81500	83200	+2.1%
Wing weight	lb_f (4.4 N)	7340	8570	+16%
Planform area	ft^2 (0.0930 m^2)	739	739	+0.0%
Fuel weight	lb_f (4.4 N)	13600	13439	−1.2%
Lift-to-drag	–	16.3	17.1	+4.9%
Volume deficit (surplus)	ft^3 (0.0283 m^3)	(60.3)	129	

The unallocated fuel volume was equal to the fuel which could be stored in a single wing of the baseline design.

When the requirement to store all the fuel in the aircraft wing is relaxed, the box-wing design can achieve superior performance compared to baseline aircraft configurations without adopting high aspect ratios. The excess fuel could be stored in the fuselage, as in Rhodes and Selberg [19], though this would require significant changes to the cabin geometry to both accommodate the extra volume and meet wheels-up landing requirements given by 14CFR§25.963(d).

5. Conclusions

The performance of box-wing aircraft was compared to conventional aircraft designed for regional-jet transport missions. Results from a parametric study which considers only the interactions between aerodynamic performance and stability show that the box-wing design has an advantage in terms of lift-to-drag ratio. A more detailed multidisciplinary study considers the additional disciplines required to predict the fuel consumption over the course of a realistic transport mission. This study also considers the effects of the mission specification on the box-wing performance.

When multiple design disciplines are considered, the box-wing design has inferior performance to conventional designs for both long- and short-range missions. The requirement to carry all the mission fuel in the aircraft wings forces the box-wing aircraft to have a significantly larger planform area, increasing the parasitic drag of the aircraft.

Opportunities exist, however, to allow the box-wing design to have superior performance to conventional aircraft. If the aircraft fuselage were designed to hold a significant fuel volume, the box-wing would have superior performance for the same mission specification. Alternatively, if the mission were changed so that the aircraft cruised at a speed below Mach 0.65, the box-wing would have an advantage in terms of fuel consumption for the long-range regional jet mission.

This rigorous comparison between conventional and box-wing aircraft used for a regional-jet transport mission identifies the conditions where box-wings had superior performance as well as the design disciplines which have the greatest effect on the performance of such designs. This study also shows the importance of considering all relevant disciplines when assessing the performance of unconventional designs to identify the critical constraints which limit the design's performance.

Conflict of interest statement

None declared.

Acknowledgements

This research was funded by the Canadian Department of National Defense contract number 18484SK123. Partial funding for the completion of the manuscript was provided from the Advanced Simulation and Computing project of the U.S. Department of Energy. Cleared for public release LA-UR-17-20514.

Appendix A. Multidisciplinary problem variables

Table A.10
Design variable names and bounds for the box-wing problem.

Variable name	Units	Lower bound passengers		Upper bound passengers		Optimal passengers	
		50	86	50	86	50	86
		Interdisciplinary coupling variables					
Maximum takeoff weight	[klb_f (4.4 kN)]	30.0	60.0	60.0	100.0	51.3	88.8
Maneuver angle of attack	[deg]	0	0	20	20	2.14	2.57
Cruise distance	[nmi (1.85 km)]	200	500	950	1540	699	1270
		Geometry variables					
Planform area	[ft^2 (0.0930 m^2)]	350	500	850	2000	727	1120
Relative fore wing area	[–]	0.2	0.2	0.8	0.8	0.500	0.493
Height-to-span ratio	[–]	0.0625	0.0625	0.5	0.5	0.308	0.250
Small wing aspect ratio	[–]	4.0	4.0	10	10	10.0	9.45
Small wing taper	[–]	0.2	0.2	1.0	1.0	0.218	0.357
Wing leading edge station[b]	[–]	0.24	0.17	0.80	0.80	0.241	0.310
Fan face station[b]	[–]	0.64	0.70	0.90	0.80	0.819	0.704
Wing segment sweeps (x3)	[deg]	0.0	0.0	60.0	60.0	48.4	45.9
						16.7	19.0
						−57.6	−50.3
Wing section twist (x6)	[deg]	−1.0	−1.0	20.0	20.0	3.68	4.66
						5.62	7.84
						7.00	2.96
						4.12	1.92
						3.00	2.03
						0.89	4.08
Fore spar location[d]	[–]	0.05	0.05	0.25	0.25	0.057	0.093
Aft spar location[e]	[–]	0.75	0.75	0.90	0.90	0.789	0.808
		Effector variables					
Main wing flap area[c]	[–]	0.0	0.0	0.3	0.3	0.00	0.024
Main wing elevator area[c]	[–]	0.0	0.0	0.3	0.3	0.151	0.120
Fore to aft flap area ratio	[–]	0.0	0.0	1.0	1.0	0.634	0.419
Fore to aft elevator area ratio	[–]	0.0	0.0	1.0	1.0	0.421	0.369
		Landing gear variables					
Main landing gear axial location[b]	[–]	0.4	0.4	0.9	0.9	0.611	0.606
Main landing gear offset[a]	[–]	0.0	0.0	1.0	1.0	0.991	0.556
Landing gear strut length	[ft (0.305 m)]	0.0	0.0	5.0	5.0	3.90	4.95
Nose gear axial location	[$/l_{fuse}$]	0.01	0.01	0.40	0.40	0.335	0.274
		Performance variables					
Maximum sea level thrust	[klb_f (4.4 kN)]	7	10	11	20	9.38	15.6
Constant CAS climb speed	[knots (1.85 km/h)]	250	250	400	400	252	254

[a] Center of gravity limits were the normalized distance between the fore and aft limits predicted by the center of gravity analysis.
[b] Normalized by fuselage length.
[c] Normalized by total planform area.
[d] Normalized by chord length.
[e] Normalized by fuselage diameter.

Table A.11
Design variable names and bounds for the baseline aircraft problem.

Variable name	Units	Lower bound passengers		Upper bound passengers		Optimal passengers	
		50	86	50	86	50	86
		Interdisciplinary coupling variables					
Maximum takeoff weight	[klb_f (4.4 kN)]	25.0	45.0	100.0	110.0	48.2	82.2
Maneuver angle of attack	[deg]	0	0	20	20	2.14	2.57
Cruise distance	[nmi (1.85 km)]	400	600	950	1540	699	1270
		Geometric variables					
Wing section twist (x3)	[deg]	0.0	−2.0	10.0	10.0	3.18	3.44
						3.57	4.30
						4.52	6.04
Winglet section twist (x2)	[deg]	−5.0	−5.0	10.0	10.0	4.86	5.38
						6.17	4.40
		Effector variables					
Takeoff stabilator, fore c.g.	[deg]	−15.0	−15.0	10.0	10.0	−9.19	−1.26
		Landing gear variables					
Main gear axial location[a]	[–]	0.410	0.458	0.585	0.611	0.585	0.609
Landing gear strut length	[ft (0.305 m)]	1.5	1.5	10.0	10.0	3.24	1.97
Nose gear axial location[a]	[–]	0.0	0.0	0.4	0.4	0.251	0.000
		Performance variables					
Maximum sea level thrust	[klb_f (4.4 kN)]	8.0	9.0	15.0	21.0	9.38	15.6
Constant CAS climb speed	[knots (1.85 km/h)]	250	250	400	400	252	254

[a] Normalized by fuselage length.

Please cite this article in press as: S.A. Andrews, R.E. Perez, Comparison of box-wing and conventional aircraft mission performance using multidisciplinary analysis and optimization, Aerosp. Sci. Technol. (2018), https://doi.org/10.1016/j.ast.2018.05.060

References

[1] I. Kroo, Nonplanar wing concepts for increased aircraft efficiency, in: Innovative Configurations and Advanced Concepts for Future Civil Aircraft, in: VKI Lecture Series, 2005.
[2] S.A. Andrews, R.E. Perez, D. Wowk, Wing weight model for conceptual design of nonplanar configurations, Aerosp. Sci. Technol. 43 (2015) 51–62, https://doi.org/10.1016/j.ast.2015.02.011.
[3] P.W. Jansen, R.E. Perez, Effect of size and mission requirements on the design optimization of non-planar aircraft configurations, in: 13th AIAA/ISSMO Multidisciplinary Analysis Optimization Conference, AIAA, Fort Worth, TX, 2010, AIAA 2010-9188.
[4] D.E. Vaughan, D.L. Preston, Physical Uncertainty Bounds (PUB), LA-UR 14-20411, Los Alamos National Laboratory, Los Alamos NM, 2014.
[5] R. Cavallaro, L. Demasi, Challenges, ideas, and innovations of joined-wing configurations: a concept from the past, an opportunity for the future, Prog. Aerosp. Sci. 87 (2016) 1–93, https://doi.org/10.1016/j.paerosci.2016.07.002.
[6] L. Prandtl, Induced Drag of Multiplanes, TN-182, NACA, Washington, DC, 1924.
[7] T. von Kármán, J.M. Burgers, General Aerodynamic Theory – Perfect Fluids, Aerodynamic Theory, vol. II, Dover, New York, NY, 1963.
[8] L. Demasi, A. Dipace, G. Monegato, R. Cavallaro, Invariant formulation for the minimum induced drag conditions of nonplanar wing systems, AIAA J. 52 (10) (2014) 2223–2240, https://doi.org/10.2514/1.J052837.
[9] D. Luciano, M. Giovanni, D. Antonio, C. Rauno, Minimum induced drag theorems for joined wings, closed systems, and generic biwings: theory, in: 56th AIAA/ASCE/AHS/ASC Structures, Structural Dynamics, and Materials Conference, AIAA, Kissimmee, FL, 2015, AIAA 2015-0697.
[10] H. Gagnon, D. Zingg, Aerodynamic optimization trade study of a box-wing aircraft configuration, in: 56th AIAA/ASCE/AHS/ASC Structures, Structural Dynamics, and Materials Conference, AIAA, Kissimmee, FL, 2015, AIAA 2015-0695.
[11] T. Chau, D.W. Zingg, Aerodynamic shape optimization of a box-wing regional aircraft based on the Reynolds-averaged Navier–Stokes equations, in: 35th AIAA Applied Aerodynamics Conference, Denver, CO, 2017, AIAA 2017-3258.
[12] D.L. Cronin, R.J. Somnay, Estimating the weight of generally configured dual wing systems, in: 26th Structures, Structural Dynamics, and Materials Conference, AIAA, Orlando, FL, 1985, pp. 173–177, AIAA 85-0641.
[13] M.F. Samuels, Structural weight comparison of a joined wing and a conventional wing, J. Aircr. 19 (6) (1982) 485–491.
[14] P.O. Jemitola, G. Monterzino, J. Fielding, Wing mass estimation algorithm for medium range box wing aircraft, Aeronaut. J. 117 (1189) (2013) 329–340, https://doi.org/10.1017/S0001924000008022.
[15] I.R. Salam, B. Cees, Multi-disciplinary analysis and optimisation methodology for conceptual design of a box-wing aircraft, Aeronaut. J. 120 (1230) (2016) 1315–1333, https://doi.org/10.1017/aer.2016.59.
[16] D. Schiktanz, D. Scholz, The conflict of aerodynamic efficiency and static longitudinal stability of box wing aircraft, in: 3rd CEAS Air & Space Conference, Venice, Italy, 2011, pp. 910–921.
[17] R. Caja, D. Scholz, Box wing flight dynamics in the stage of conceptual aircraft design, in: Deutscher Luft- und Raumfahrtkongress, 2012, 281383.
[18] J. Wolkovitch, The joined wing: an overview, J. Aircr. 23 (3) (1986) 161–178.
[19] M.D. Rhodes, B.P. Selberg, Dual wing, swept forward swept rearward wing and single wing design optimization for high performance business airplanes, in: 13th Congress of the International Council of the Aeronautical Sciences, Seattle, WA, 1982, pp. 496–511.
[20] G. Iezzi, PrandtlPlane High Lift System Preliminary Aerodynamic Design, Ph.D. thesis, Università Di Pisa, Pisa Italy, 2005.
[21] S.A. Andrews, R.E. Perez, Parametric Study of Box-Wing Aerodynamic Design for Minimum Drag Under Stability and Maneuverability Constraints, in: 33rd AIAA Applied Aerodynamics Conference, AIAA, Dallas, TX, 2015, AIAA 2015-3291.
[22] P. Jackson (Ed.), All the World's Aircraft, Jane's Information Group Ltd., Surrey, UK, 2004.
[23] S.A. Andrews, R.E. Perez, Analytic study of the conditions required for longitudinal stability of dual-wing aircraft, Proc. Inst. Mech. Eng., Part G, J. Aerosp. Eng. 232 (5) (2018) 958–972, https://doi.org/10.1177/0954410017704215.
[24] W.F. Phillips, Mechanics of Flight, 1st edition, John Wiley & Sons, Hoboken, NJ, 2004.
[25] D.P. Raymer, Aircraft Design: A Conceptual Approach, AIAA Education Series, AIAA, Washington, DC, 1992.
[26] G.P. Murray, M. Saunders, SNOPT: an SQP algorithm for large-scale constraint optimization, SIAM J. Optim. 12 (4) (2002) 979–1006, https://doi.org/10.1137/S0036144504446096.
[27] R.E. Perez, P.W. Jansen, J.R.R.A. Martins, pyOpt: a Python-based object-oriented framework for nonlinear constrained optimization, Struct. Multidiscip. Optim. 45 (1) (2012) 101–118, https://doi.org/10.1007/s00158-011-0666-3.
[28] P.W. Jansen, Robust Coupled Optimization of Aircraft Family Design and Fleet Allocation for Multiple Markets, Ph.D. thesis, Royal Military College of Canada, Kingston, ON, Mar. 2015, http://hdl.handle.net/11264/562.
[29] M.M. Munk, General Biplane Theory, Report 151, NACA, Washington, DC, 1923.
[30] J. Roskam, Preliminary Sizing of Airplanes, Airplane Design, vol. 1, DAR Corporation, Lawrence, KS, 2005.
[31] S.A. Andrews, Multidisciplinary Analysis of Closed, Nonplanar Wing Configurations for Transport, Aircraft, Ph.D. Thesis, Royal Military College of Canada, Kingston, ON, Apr. 2016, http://hdl.handle.net/11264/1002.
[32] S.A. Powers, Critical field length calculations for preliminary design, AIAA J. Aircr. 18 (2) (1981) 103–107, https://doi.org/10.2514/3.44698.
[33] S. Gallay, E. Laurendeau, Preliminary-design aerodynamic model for complex configurations using lifting-line coupling algorithm, J. Aircr. 53 (4) (2016) 1145–1154, https://doi.org/10.2514/1.C033460.
[34] J. Katz, A. Plotkin, Low Speed Aerodynamics, 1st edition, McGraw-Hill, Singapore, 1991.
[35] O. Gur, W.H. Mason, J.A. Schetz, Full-configuration drag estimation, J. Aircr. 47 (4) (2010) 1356–1367, https://doi.org/10.2514/1.47557.
[36] S.A. Andrews, R.E. Perez, Stability and control effects on the design optimization of a box-wing aircraft, in: 14th AIAA Aviation Technology, Integration, and Operations Conference, Atlanta, GA, 2014, 2014-2592.
[37] H.J. Morgan, J.W. Paulson, Low-Speed Aerodynamic Performance of a High-Aspect-Ratio Supercritical-Wing Transport Model Equipped With Full-Span Slat and Part-Span Double-Slotted Flaps, TP 1580, NASA, Washington, DC, 1979.
[38] Engineering Sciences Data Unit, VGK Method for Two-Dimensional Aerofoil Sections Part 1: Principles and Results, ESDU 96028, 1996.
[39] J. Roskam, Preliminary Calculation of Aerodynamic, Thrust and Power Characteristics, Airplane Design, vol. 6, DAR Corporation, Lawrence, KS, 2008.
[40] A.B. Lambe, J.R. Martins, Extensions to the design structure matrix for the description of multidisciplinary design, analysis, and optimization processes, Struct. Multidiscip. Optim. 46 (2) (2012) 273–284, https://doi.org/10.1007/s00158-012-0763-y.
[41] M. Bartel, T.M. Young, Simplified thrust and fuel consumption models for modern two-shaft turbofan engines, AIAA J. Aircr. 45 (4) (2008) 1450–1456, https://doi.org/10.2514/1.35589.
[42] J.D. Mattingly, Elements of Gas Turbine Propulsion, 1st edition, McGraw-Hill Mechanical Engineering, McGraw-Hill, 1996.
[43] B.H. Oman, Vehicle Design Evaluation Program, CR 145070, NASA, Washington, DC, 1977.
[44] L.A. McCullers, Aircraft configuration optimization including optimized flight profiles, in: J. Sobieski (Ed.), Symposium on Recent Experiences in Multidisciplinary Analysis and Optimization, NASA, Hampton, VA, 1984.
[45] R.E. Perez, A Multidisciplinary Optimization Framework for Flight Dynamics and Control Integration in Aircraft Design, Ph.D. Thesis, University of Toronto, Toronto, ON, Canada, 2007.
[46] M.N. Beltramo, D.L. Trapp, B.W. Kimoto, D.P. Marsh, Parametric Study of Transport Aircraft Cost and Weight, CR 151970, NASA, Washington, DC, 1977.
[47] S. Chai, P. Crisafuli, W.H. Mason, Aircraft center of gravity estimation in conceptual design, in: Aircraft Engineering, Technology, and Operations Congress, AIAA, Los Angeles, CA, 1995, AIAA 95-3882.
[48] J. Roskam, Determination of Stability, Control and Performance Characteristics: FAR and Military Requirements, Airplane Design, vol. 7, DAR Corporation, Lawrence, KS, 2006.
[49] E.J. Cramer, J.E. Dennis, P.D. Frank, R.M. Lewis, G. Shubin, Problem formulation for multidisciplinary optimization, SIAM J. Control Optim. 4 (4) (1994) 754–776, https://doi.org/10.1137/0804044.
[50] Federal Aviation Administration, Airport Design, Advisory Circular, AC 150/5300-13A, U.S. Department of Transportation, Washington, DC, 2014.
[51] N.S. Currey, Aircraft Landing Gear Design: Principles and Practices, AIAA Education Series, AIAA, Washington, DC, 1988.
[52] C. Gedeon, T.T. Takahashi, Multi-disciplinary survey of engine parameters and its impact on performance and energy maneuverability, in: 14th AIAA Aviation Technology, Integration, and Operations Conference, AIAA, Atlanta, GA, 2014, AIAA 2014-2032.

Please cite this article in press as: S.A. Andrews, R.E. Perez, Comparison of box-wing and conventional aircraft mission performance using multidisciplinary analysis and optimization, Aerosp. Sci. Technol. (2018), https://doi.org/10.1016/j.ast.2018.05.060